First-principles-driven Control of the Rotational Transform Profile in High Performance Discharges in the DIII-D Tokamak

Wenyu Shi, Justin E. Barton, William Wehner, Mark D. Boyer, Arnold Kritz and Eugenio Schuster

***Abstract*— In this work, a first-principles-driven, control-oriented, nonlinear, partial-differential-equation model of the poloidal flux profile evolution is utilized to design a feedback control algorithm to regulate the rotational transform profile in the DIII-D tokamak. The control goal is to regulate the rotational transform profile, which is related to the poloidal flux profile, around a particular target profile. A singular value decomposition of the nominal plasma model at steady state is carried out to decouple the system and identify the most relevant control channels. A mixed sensitivity H_∞ control design problem is formulated to synthesize a stabilizing feedback controller to minimize the reference tracking error with minimal control energy. Simulations based on the first-principles-driven model show that the H_∞ controller is capable of regulating the system around the target ι profile in the presence of disturbances. When compared to a previously designed data-driven model-based controller, the proposed first-principles-driven model-based controller shows potential for improving the control performance.**

I. Introduction

The tokamak is a high order, distributed parameter, nonlinear system with a large number of instabilities, and even under restrictive assumptions the poloidal flux profile, or equivalently current profile, models are highly nonlinear and based on partial differential equations (PDEs). The complexity of these first-principles models needs to be reduced to facilitate design of compact and reliable control strategies. During the model simplification process, there is always a trade-off between the simplicity of the model and both its physics accuracy and range of validity. First-principles-driven modeling provides the freedom of arbitrarily handling this trade-off and deciding on the level of simplicity, accuracy and validity of the model. Several first-principles-driven, control-oriented, PDE models have been recently proposed for current profile control [1], [2], [3]. The model developed for DIII-D [1] is valid for low-confinement (L-mode) discharges, and has been used to determine optimal feedforward actuator trajectories that achieve and sustain a desired current profile [4]. The model has also been used to design complementing feedback controllers that add robustness against disturbances and model uncertainties, which have been experimentally tested in DIII-D [5], [6], [7].

In this work, we extend our previous work by developing first-principles-driven feedback controllers for current profile regulation in high-confinement (H-mode) scenarios. Firstly, the first-principles-driven model of the current profile evolution is extended from L-mode to H-mode. Additionally, the effects of the actuators are modeled independently, instead of lumping them into a single input [8]. Secondly, a singular value decomposition [9] of the static gain matrix of the nominal plant model is employed to determine which linear combinations of the plant outputs we can effectively control. The mixed sensitivity H_∞ control method is then applied to synthesize a closed-loop controller that minimizes the reference tracking error and rejects external disturbances with minimal control energy. Finally, the control performances of the first-principles-driven model-based controller and a previously designed data-driven model-based controller [10] are compared.

This paper is organized as follows. In Section II, a first-principles-driven model for the poloidal flux profile evolution is presented. In Section III, the PDE model is linearized around the feedforward trajectories of the system. Based on the linear state-space model, the design of the plasma control algorithm is described. Closed-loop simulated and the comparison results are presented in Section IV. Section V states the conclusions.

II. Current Profile Evolution Model on DIII-D

The evolution of the poloidal magnetic flux is defined by the magnetic diffusion equation [11], which is expressed as

$$\frac{\partial \psi}{\partial t} = \frac{f_1 u_1(t)}{\hat{\rho}} \frac{\partial}{\partial \hat{\rho}} (\hat{\rho} D_\psi \frac{\partial \psi}{\partial \hat{\rho}}) + \sum_{i=2}^{15} f_i u_i(t) + (\frac{\partial \psi}{\partial \hat{\rho}})^{-1} f_{16} u_{16}(t), \tag{1}$$

with boundary conditions:

$$\frac{\partial \psi}{\partial \hat{\rho}}|_{\hat{\rho}=0} = 0, \quad \frac{\partial \psi}{\partial \hat{\rho}}|_{\hat{\rho}=1} = -k_{17} u_{17}(t),$$

where

$$D_\psi = \hat{F}\hat{G}\hat{H}, \quad k_{17} = \frac{\mu_0}{2\pi} \frac{R_0}{\hat{G}|_{\hat{\rho}=1} \hat{H}|_{\hat{\rho}=1}}.$$

The parameter ψ is the poloidal stream function which is related to the poloidal flux Ψ, i.e., $\Psi = 2\pi\psi$. The parameter μ_0 is the vacuum permeability, and the parameter $\hat{\rho}$ is the normalized effective minor radius, which is denoted as $\hat{\rho} = \frac{\rho}{\rho_b}$, where ρ is the mean effective minor radius of the flux surface, i.e., $\pi B_{\phi,0} \rho^2 = \Phi$. The parameter Φ is the toroidal magnetic flux, and $B_{\phi,0}$ is the magnetic field at the geometric major radius R_0. The parameter ρ_b is the effective minor radius of the last closed magnetic flux surface. The parameters $\hat{F}$, $\hat{G}$ and $\hat{H}$ are geometric factors pertaining to the magnetic configuration of a particular plasma equilibrium,

This work was supported by the National Science Foundation CAREER Award program (ECCS-0645086), and the U.S. Department of Energy (DE-FG02-09ER55064 and DE-FC02-04ER54698). W. Shi (wenyu.shi@lehigh.edu), J.E. Barton, W. Wehner, M.D. Boyer and E. Schuster are with the Department of Mechanical Engineering & Mechanics, Lehigh University, Bethlehem, PA 18015. A. Kritz is with the Department of Physics, Lehigh University, Bethlehem, PA 18015.

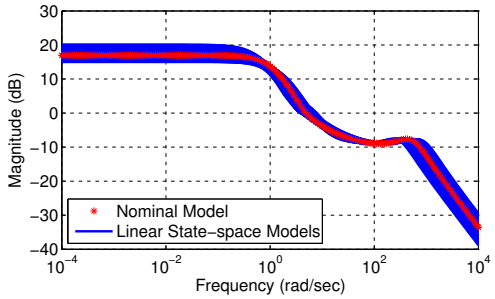

Fig. 1. Frequency response of first-principles-driven plasma models.

and $f_1, f_2, \cdots, f_{16}$ are functions of the radial coordinate $\hat{\rho}$ [8]. The inputs in (1) are expressed as:

$$u_1 = \frac{u_n^{3/2}}{(I_p\sqrt{P_{tot}})^{3/2}}, \quad u_{i+1} = \frac{P_{ec_i}}{(I_p\sqrt{P_{tot}})^{1/2}u_n^{1/2}}, \tag{2}$$

$$u_{j+7} = \frac{P_{nbi_j}}{(I_p\sqrt{P_{tot}})^{1/2}u_n^{1/2}}, \; u_{16} = \frac{u_n^{3/2}}{(I_p\sqrt{P_{tot}})^{1/2}}, \; u_{17} = I_p,$$

where $i \in \{1,2,\cdots,6\}$ and $j \in \{1,2,\cdots,8\}$. The parameter u_n regulates time evolution of the electron density, and I_p is the plasma current. The parameter P_{tot} is the total power injected into the plasma, the parameters P_{ec_i} and P_{nbi_j} are the power injected from the individual launchers of the EC system and NBI system respectively.

The rotational transform ι profile, defined as $\iota(\hat{\rho},t) = -d\Psi/d\Phi$, is written as

$$\iota(\hat{\rho},t) = -\frac{d\Psi}{d\Phi} = -\frac{2\pi\frac{\partial\psi}{\partial\hat{\rho}}}{\frac{\partial\Phi}{\partial\rho}\frac{\partial\rho}{\partial\hat{\rho}}} = -\frac{\theta}{B_{\phi,0}\rho_b^2\hat{\rho}} \triangleq C_{FP}(\hat{\rho})\theta, \tag{3}$$

where $\theta(\hat{\rho},t) = \frac{\partial\psi}{\partial\hat{\rho}}(\hat{\rho},t)$ is the gradient of the poloidal flux profile. Therefore, we develop a model for θ, so we can control the ι profile evolution. Using the chain rule, (1) is expanded as

$$\frac{\partial\psi}{\partial t} = \frac{f_1u_1}{\hat{\rho}}(\hat{\rho}\frac{\partial\psi}{\partial\hat{\rho}}\frac{dD_\psi}{d\hat{\rho}} + D_\psi\frac{\partial\psi}{\partial\hat{\rho}} + \hat{\rho}D_\psi\frac{\partial^2\psi}{\partial\hat{\rho}^2}) + \sum_{i=2}^{15} f_iu_i + (\frac{\partial\psi}{\partial\hat{\rho}})^{-1}f_{16}u_{16}. \tag{4}$$

By differentiating (4) with respect to $\hat{\rho}$, the PDE governing the evolution of $\theta(\hat{\rho},t)$ is found to be

$$\frac{\partial\theta}{\partial t} = (h_{11}\frac{\partial^2\theta}{\partial\hat{\rho}^2} + h_{12}\frac{\partial\theta}{\partial\hat{\rho}} + h_{13}\theta)u_1(t) + \sum_{i=2}^{15}\frac{df_i}{d\hat{\rho}}u_i(t) + (\frac{1}{\theta}\frac{df_{16}}{d\hat{\rho}} - \frac{f_{16}}{\theta^2}\frac{\partial\theta}{\partial\hat{\rho}})u_{16}(t), \tag{5}$$

with boundary condition

$$\theta(0,t) = 0, \qquad \theta(1,t) = -k_{17}u_{17}(t),$$

where $h_{11} = f_1D_\psi$, $h_{12} = \frac{f_1D_\psi}{\hat{\rho}} + f_1'D_\psi + 2f_1D_\psi'$, and $h_{13} = f_1'D_\psi' + f_1D_\psi'' + \frac{f_1'D_\psi}{\hat{\rho}} + \frac{f_1D_\psi'}{\hat{\rho}} - \frac{f_1D_\psi}{\hat{\rho}^2}$.

In this work, DIII-D shot #146419 is chosen as the reference shot, and PTRANSP [12] analyzed results of this shot are employed to identify the reference profiles and constants needed to complete the control-oriented models presented above. More details on the modeling approach can be found in the companion paper [8].

III. Control System Design

In this section, a multi-input-multi-output (MIMO) feedback controller based on the first-principles-driven model (3)-(5) is proposed for the regulation of the evolution of the ι profile on DIII- D.

A. Model Reduction and Linearization

The model (5) is discretized in space using a truncated Taylor series expansion to approximate the spatial derivatives to construct a reduced-order model suitable for control design. The non-dimensional domain of interest, $[0,1]$, is represented as l nodes, and the spacing between the nodes, $\Delta\hat{\rho}$, is defined as $\Delta\hat{\rho} = 1/(l-1)$. Central finite difference spatial derivative approximations of $O(\Delta\hat{\rho}^2)$ are used in the interior node region, $2 \le i \le (l-1)$. The reduced-order discretized model is expressed as

$$\dot{X} = W(X,u), \tag{6}$$

where $X = [\theta_2, \theta_3, \cdots, \theta_{l-1}]^T$, $u = [u_1, u_2, \cdots, u_{17}]^T$, and W is a nonlinear function of the states and inputs. Let X_{FF}, u_{FF} and y_{FF} be the feedforward trajectories of the states, inputs and outputs, and these feedforward trajectories satisfy

$$\dot{X}_{FF} = W(X_{FF}, u_{FF}), \quad y_{FF} = C_{FP}X_{FF}. \tag{7}$$

By defining the perturbation variables $x = X - X_{FF}$ and $\Delta u = u - u_{FF}$, a linear model suitable for tracking control design can be obtained. Inserting the perturbation variables into (6) results in

$$\dot{X}_{FF} + \dot{x} = W|_{X_{FF},u_{FF}} + \frac{\partial W}{\partial X}|_{X_{FF},u_{FF}}x + \frac{\partial W}{\partial u}|_{X_{FF},u_{FF}}\Delta u + \cdots$$

Ignoring the higher order terms, a series of linear models are expressed as:

$$\dot{x} = \frac{\partial W}{\partial X}|_{X_{FF},u_{FF}}x + \frac{\partial W}{\partial u}|_{X_{FF},u_{FF}}\Delta u = A_{FP}(t)x + B_{FP}(t)\Delta u.$$

By defining the outputs $\Delta y = y - y_{FF}$, we can obtain

$$y_{FF} + \Delta y = C_{FP}(X_{FF} + x).$$

Therefore, we obtain a linear time-variant, dynamic, state-space model, i.e.,

$$\dot{x} = A_{FP}(t)x + B_{FP}(t)\Delta u, \quad \Delta y = C_{FP}x. \tag{8}$$

A frequency study of the family of the state-space models (8) for $t = 0.5s$ to $t = 6s$, which compares the maximum singular values of the time-variant ι profile models, shows that the models do not have a large magnitude difference, as shown in Fig. 1. Based on this frequency study, the model at 1.75 s is chosen as the nominal model P_{FP_0}, i.e.,

$$\dot{x} = A_{FP_0}x + B_{FP_0}\Delta u, \quad \Delta y = C_{FP_0}x. \tag{9}$$

The feedback controller is designed based on (9).

B. Singular Value Decomposition

Assuming a constant target $\Delta\bar{y}_{tar}$ and closed-loop stabilization, the system will reach steady state as $t \to \infty$. It is possible to define $\Delta\bar{y} = \lim_{t\to\infty}\Delta y(t)$, $\Delta\bar{u} = \lim_{t\to\infty}\Delta u(t)$, and $\bar{e} = \lim_{t\to\infty}e(t) = \Delta\bar{y}_{tar} - \Delta\bar{y}$. Therefore, the closed-loop system in steady state is specified by

$$\Delta\bar{y} = \bar{P}_{FP_0}\Delta\bar{u} = -C_{FP_0}A_{FP_0}^{-1}B_{FP_0}\Delta\bar{u}, \quad \Delta\bar{u} = \bar{K}\bar{e},$$

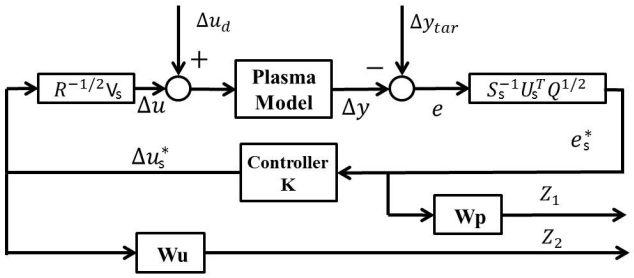

Fig. 2. H_∞ control formulation.

where $P_{FP_0}(s)$ is the transfer function of (9) and $\bar{P}_{FP_0} = P_{FP_0}(0)$, and $\hat{K}(s)$ represents the transfer function of the to-be-designed controller and $\bar{\hat{K}} = \hat{K}(0)$.

In order to weight the control effort and tracking error, two positive definite weighting matrices $R \in \Re^{m\times m}$ and $Q \in \Re^{p\times p}$ are introduced to the system, where $p = l-2$ is the number of outputs and m is the number of inputs. We then define the "weighted" steady-state transfer function, and its singular value decomposition (SVD) as $\tilde{P}_{FP_0} = Q^{1/2}\bar{P}_{FP_0}R^{-1/2} = USV^T$, where $S = \text{diag}(\sigma_1, \sigma_2, \cdots, \sigma_m) \in \Re^{m\times m}$, $U \in \Re^{p\times m}$ ($U^TU = I$), and $V \in \Re^{m\times m}$ ($V^TV = VV^T = I$). By invoking the properties of the SVD, the matrix $Q^{-1/2}US$ defines a basis of the steady-state output values, and the matrix $R^{-1/2}V$ defines a basis of the steady-state input values. By defining $\Delta\bar{y}^* = S^{-1}U^TQ^{1/2}\Delta\bar{y}$, $\Delta\bar{y}^*_{tar} = S^{-1}U^TQ^{1/2}\Delta\bar{y}_{tar}$, and $\Delta\bar{u}^* = V^TR^{1/2}\Delta\bar{u}$, a square decoupled system is obtained:

$$\Delta\bar{y}^* = S^{-1}U^TQ^{1/2}\Delta\bar{y} = S^{-1}U^TQ^{1/2}Q^{-1/2}USV^TR^{1/2}\Delta\bar{u} = \Delta\bar{u}^*.$$

Substituting these expressions into the performance index $\bar{J} = \bar{e}Q\bar{e}^T$, the steady state cost function is obtained as:

$$\bar{J} = (\Delta\bar{y}^*_{tar} - \Delta\bar{y}^*)^T S^2(\Delta\bar{y}^*_{tar} - \Delta\bar{y}^*) = \sum_{i=1}^{m}\sigma_i^2(\Delta\bar{y}^*_{tar_i} - \Delta\bar{y}^*_i)^2.$$

It is usually the case where $\sigma_1 > \cdots \sigma_k \gg \sigma_{k+1} > \cdots > \sigma_m > 0$. To avoid spending a lot of control effort for a marginal improvement of the cost function value, we partition the singular value set into significant singular values S_s and negligible singular values S_n. We can write $U = \begin{bmatrix} U_s & U_n \end{bmatrix}$, $V = \begin{bmatrix} V_s & V_n \end{bmatrix}$, $S = \text{diag}(S_s, S_n)$, and approximate the cost function $\bar{J}$ by

$$\bar{J}_s = \sum_{i=1}^{k}\sigma_i^2(\Delta\bar{y}^*_{tar_i} - \Delta\bar{y}^*_i)^2 = (\Delta\bar{y}^*_{tar_s} - \Delta\bar{y}^*_s)^T S_s^2(\Delta\bar{y}^*_{tar_s} - \Delta\bar{y}^*_s),$$

where $\Delta\bar{y}^*_{tar_s} = S_s^{-1}U_s^TQ^{1/2}\Delta\bar{y}_{tar}$, $\Delta\bar{y}^*_s = S_s^{-1}U_s^TQ^{1/2}\Delta\bar{y}$, $\bar{e}^*_s = \Delta\bar{y}^*_{tar_s} - \Delta\bar{y}^*_s$ and $\Delta\bar{u}^*_s = V_s^TR^{1/2}\Delta\bar{u}$. The matrix bases reduce to $Q^{-1/2}U_sS_s$ and $R^{-1/2}V_s$, and the decoupled system,

$$P_{FP_{DC}} = S_s^{-1}U_s^TQ^{1/2}P_{FP_0}R^{-1/2}V_s, \tag{10}$$

represents a one-to-one relationship at steady state between the inputs $\Delta\bar{u}^*_s$ and the outputs $\Delta\bar{y}^*_s$. More details of SVD can be found in our previous work [10].

C. Design of Mixed Sensitivity H_∞ Controller

The mixed sensitivity H_∞ technique is used to design the plasma ι profile controller, which can minimize the tracking error $e(t)$ while using as little feedback control effort as possible. The structure of the proposed controller is shown in Fig. 2, where K is the feedback controller, Δu_d is the input disturbance, $Z_1 = W_pe^*_s$, $Z_2 = W_u\Delta u^*_s$, and W_p and W_u are two frequency-dependent weighting functions. The feedback system shown in Fig. 2, is expressed in the conventional $P^* - K$ control framework. The generalized plant P^* is the transfer function from the input signals $[\Delta y^{*T}_{tar_s}, \Delta u^{*T}_s]^T$ to the output signals $[Z_1^T, Z_2^T, e^{*T}_s]^T$, where $\Delta u^*_s = V_s^TR^{1/2}\Delta u$, $\Delta y^*_{tar_s} = S_s^{-1}U_s^TQ^{1/2}\Delta y_{tar}$, $\Delta y^*_s = S_s^{-1}U_s^TQ^{1/2}\Delta y$, and $e^*_s = \Delta y^*_{tar_s} - \Delta y^*_s$. The closed-loop transfer function is given by the lower linear fractional transformation (LFT), i.e.,

$$T_{zw} = F_l(P^*, K) = \begin{bmatrix} W_pM_s \\ W_uKM_s \end{bmatrix}, \tag{11}$$

where the sensitivity transfer function M_s is defined as $M_s = (I + P_{FP_{DC}}K)^{-1}$. Our purpose is to seek a controller $K(s)$ that stabilizes the system and minimizes the H_∞ norm of the transfer function T_{zw}, i.e.,

$$\min_{K(s)}\|T_{zw}(P^*, K)\|_\infty = \min_{K(s)}(\sup_\omega \bar{\sigma}[T_{zw}(P^*, K)(j\omega)]),$$

where $\bar{\sigma}$ represents the maximum singular value. This statement defines a mixed sensitivity H_∞ control problem, and the goal is to minimize both the tracking error (W_pM_s) and the control effort (W_uKM_s) at the same time. The weighting functions $W_p = \text{diag}\{W_{p_i}\}$ and $W_u = \text{diag}\{W_{u_i}\}$ are

$$W_{p_i}(s) = (\frac{s/\sqrt{M_{p_i}} + \omega_{p_i}}{s + \omega_{p_i}\sqrt{H_{p_i}}})^2, \quad W_{u_i}(s) = (\frac{s + \omega_{u_i}\sqrt{H_{u_i}}}{s/\sqrt{M_{u_i}} + \omega_{u_i}})^2,$$

where the coefficients M_{p_i}, ω_{p_i}, H_{p_i}, M_{u_i}, ω_{u_i}, and H_{u_i}, for $i = 1, 2, \cdots, k$, are design parameters in the H_∞ control synthesis. Finally, the overall plasma rotational transform ι profile controller can be written as

$$\hat{K}(s) = \frac{\Delta U(s)}{E(s)} = R^{-1/2}V_sK(s)S_s^{-1}U_s^TQ^{1/2}, \tag{12}$$

where $\Delta U(s)$ and $E(s)$ denotes the Laplace transform of Δu and e respectively.

D. Nonlinear Transformation

The outputs of the controller (12) now need to be converted to the physical actuator signals, I_p, P_{ec_i}, P_{nbi_j}, and u_n by nonlinearly inverting (3). However, there are eight beams in NBI, six gyrotrons in EC, plasma current I_p and density evolution parameter u_n, totaling only sixteen independent actuators in DIII-D, but there are seventeen inputs in (5). Therefore, it is impossible to obtain a unique relationship between u in (5) and the physical actuator signals.

There are two different types of NBI beams in DIII-D: co-current and counter-current injection, which allows an important capability of mixed co-injection and counter-injection to heat the plasma without driving current. Based on this capability, a new variable representing the fraction of power generating heat but not driving current, and denoted as balanced-beam NBI power P_{BL}, is introduced in the model. The beam power P_{nbi_i} is therefore expressed as $P_{nbi_i} = P_{nbi_{i,CD}} + \gamma_{nbi_i}P_{BL}$, with $i \in \{1, 2, \cdots, 8\}$, where $P_{nbi_{i,CD}}$ is the portion of the NBI power that drives current and γ_{nbi_i} is the fraction of balanced-beam NBI power contributed by each beam. The objective is to determine the γ_{nbi_i} for each beam that minimizes the non-inductive current driven by P_{BL}. This defines a constrained linear optimal control problem,

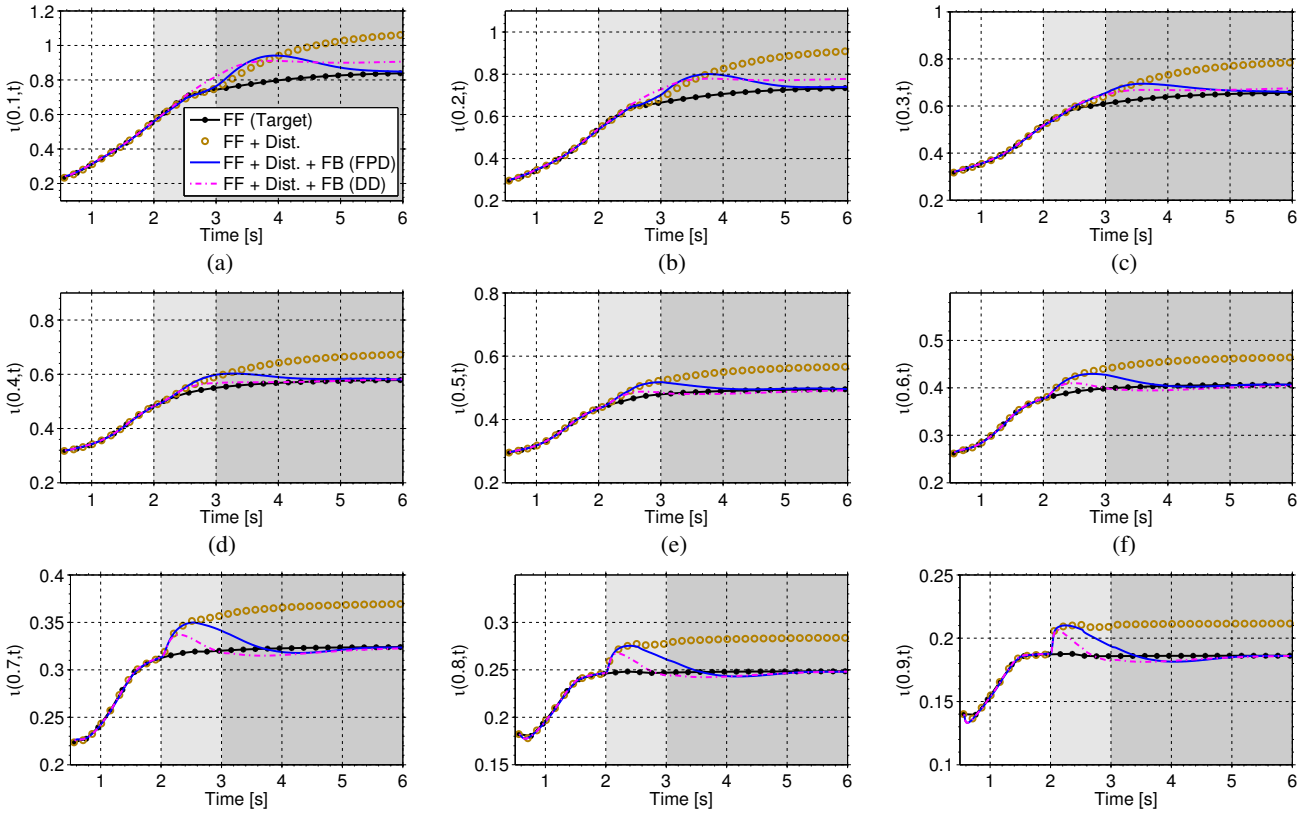

Fig. 3. Rotational transform ι Profile closed-loop simulated outputs at $\hat{\rho} = 0.1$, 0.2, 0.3, 0.4, 0.5, 0.6, 0.7, 0.8, 0.9: Reference (feedforward) outputs (black solid-dotted lines), feedforward outputs with disturbances (brown circle line), feedforward+feedback outputs by first-principles-driven (FPD) controller (blue solid lines), and feedforward+feedback outputs by data-driven (DD) controller (magenta dashed-dotted lines). White background: feedback on - disturbance off; light-gray background: feedback on - Disturbance I on; dark-gray background: feedback on - Disturbance II on.

$$\min_{\gamma_{nbi_i}} J_{BL}, \text{ s.t. } \sum_{i=1}^{8} \gamma_{nbi_i} = 1, \tag{13}$$

where J_{BL} is a cost function, defined as

$$J_{BL} = \int_0^1 \left(\sum_{i=1}^{8} \tilde{j}_{nbi_i}^{dep}(\hat{\rho}) \gamma_{nbi_i} P_{BL} \right)^2 d\hat{\rho}, \tag{14}$$

and where $\tilde{j}_{nbi_i}^{dep}$ is the normalized deposition profile, defined as $\tilde{j}_{nbi_i}^{dep} = j_{nbi_i}^{dep} / P_{nbi_i}$. The parameter $j_{nbi_i}^{dep}$ is a reference deposition profile for the i^{th} beam of NBI (see [8]).

The total power P_{tot} in DIII-D is expressed as $P_{tot} = P_{ohm} + \sum_{i=1}^{6} P_{ec_i} + \sum_{i=1}^{8} P_{nbi_i} - P_{rad}$. The ohmic power P_{ohm} and the radiated power P_{rad} are typically small, and can be neglected when compared with the injected NBI and EC power, i.e.,

$$P_{tot} \approx \sum_{i=1}^{6} P_{ec_i} + \sum_{i=1}^{8} P_{nbi_i} = \sum_{i=1}^{6} P_{ec_i} + \sum_{i=1}^{8} P_{nbi_{i,CD}} + P_{BL}.$$

Therefore, the inverse nonlinear transformation between the inputs in (5) and the physical actuators are

$$I_p = u_{17}, \quad P_{ec_i} = \frac{u_{i+1} u_{16}}{u_1^{2/3}}, \quad P_{nbi_{j,CD}} = \frac{u_{j+7} u_{16}}{u_1^{2/3}},$$

$$P_{BL} = \left(\frac{u_{16}}{u_1 u_{17}}\right)^2 - \sum_{k=2}^{15} \frac{u_k u_{16}}{u_1^{2/3}}, \quad u_n = \frac{u_{16}}{u_1^{2/3}}, \tag{15}$$

where $u_l = u_{FF_l} + \Delta u_l$, $i \in \{1,2,\cdots,6\}$, $j \in \{1,2,\cdots,8\}$, and $l \in \{1,2,\cdots,17\}$.

IV. Closed-loop Simulations and Comparison

The closed-loop simulations in this section are based on the first-principles-driven (FPD) magnetic diffusion equation (1), which predicts the poloidal magnetic flux profile evolution during H-mode discharge in DIII-D [8]. The reference plasma current, density evolution parameter, and heating and current drive (H&CD) powers are obtained from the feedforward shot #146417 and denoted as u_{FF}. The ι profile resulting from these reference (feedforward) inputs, denoted as y_{FF}, is used as target in this simulation study. Both u_{FF} and y_{FF} are represented by black dotted lines in the figures in this section. Based on the present pulse capability of the EC system in DIII-D, the EC power is turned on at $t = 2.5$ s. Two different disturbances $\Delta u_{d_i} = [\Delta I_{p_d}, \Delta P_{ec_{j,d}}, \Delta P_{nbi_{k,d}}, \Delta u_{n_d}]$, shown in Table I, are introduced in the simulation, where $i \in \{1,2\}$, $j \in \{1,\cdots,6\}$, and $k \in \{1,\cdots,8\}$. Disturbance I, Δu_{d_1}, representing a relatively large disturbance (0.1 MA) in I_p and small total disturbance (0.5 MW) in the NBI, is introduced at $t = 2$ s. Disturbance II, Δu_{d_2}, representing a relatively large disturbance (0.1 MA) in I_p and large total disturbance (1 MW) in the NBI and EC, is introduced at $t = 3$ s. The start time of the feedback controlled phase is 0.5 s. The performance of the proposed first-principles-driven (FPD) controller is compared with the performance of a previously designed data-driven (DD) controller [10]. The closed-loop-controlled ι profile (blue solid lines by the

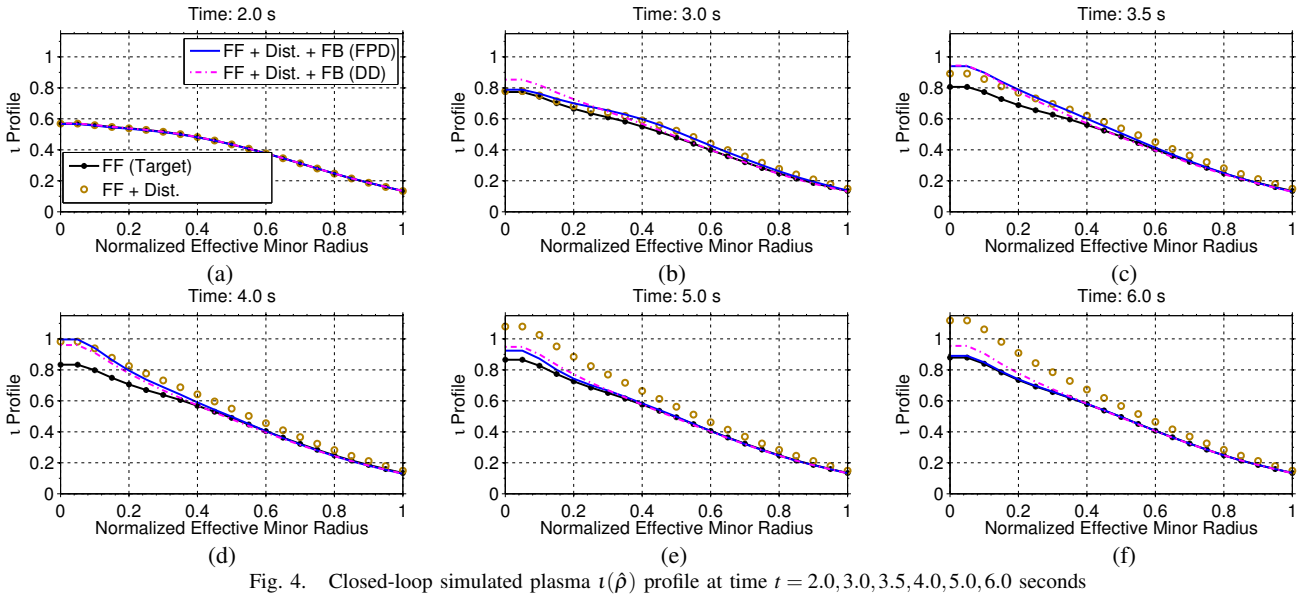

Fig. 4. Closed-loop simulated plasma $\iota(\hat{\rho})$ profile at time $t = 2.0, 3.0, 3.5, 4.0, 5.0, 6.0$ seconds

TABLE I

INPUT DISTURBANCES (UNITS: MA & MW)

Dis.	ΔI_{p_d}	$\Delta P_{ec_{1_d}}$	$\Delta P_{ec_{2_d}}$	$\Delta P_{ec_{3_d}}$	$\Delta P_{ec_{4_d}}$	$\Delta P_{ec_{5_d}}$	$\Delta P_{ec_{6_d}}$	$\Delta P_{nbi_{3_d}}$	$\Delta P_{nbi_{4_d}}$	$\Delta P_{nbi_{5_d}}$	$\Delta P_{nbi_{7_d}}$	$\Delta P_{nbi_{8_d}}$	Δu_{n_d}
Δu_{d_1}	0.1	0	0	0	0	0	0	-0.25	-0.25	0	0	0	0
Δu_{d_2}	0.1	-0.1	-0.1	-0.25	-0.25	-0.1	-0.2	-0.25	-0.25	0	-0.25	-0.25	0

first-principles-driven (FPD) controller, and magenta dashed-dotted lines by the data-driven (DD) controller [10]) at $\hat{\rho} =$ 0.1, 0.2, 0.3, 0.4, 0.5, 0.6, 0.7, 0.8, 0.9 are shown in Fig. 3. In addition, the feedforward (target) outputs (black solid-dotted lines) and feedforward with disturbances (brown circle lines) are shown in the same figure. In order to keep the outer profile tracking errors small, the plasma current disturbance is quickly rejected by the FPD and DD controllers after $t = 3$ s. There are nearly no tracking errors after $t = 4$ s for ι at $\hat{\rho} \geq 0.4$ as noted from Fig. 3 (d)-(i). Note that the inner ι profile response is much slower than the boundary ι profile response, which is due to the high temperature and slow diffusivity in the core relative to the boundary. This effect is explicitly taken into account by including the temperature profile model in the FPD model. In the data-driven approach [10], system identification technique assumes the limited bandwidth for the ι profile response, which may pose a risk to closed-loop performance due to the neglected dynamics. Comparing with the DD controller, the control performance of the FPD controller to the inner part of the ι profile ($\hat{\rho} \leq 0.2$) is improved, as shown in Fig. 3 (a)-(b). A series of six plasma ι profiles at different times during the simulation are shown in Fig. 4. The black solid-dotted lines denote the target profiles, and we see that with feedforward-only control the target profile is not achieved in the presence of the disturbance (brown circle lines). Improved performance can be observed by comparing FPD (blue solid lines) and DD (magenta dashed-dotted lines) controlled outputs. More specifically, the closed-loop simulated results by the first-principles-driven model-based controller in Fig. 3 and Fig. 4 show control performance improvement in the inner part of the ι profile.

The closed-loop outputs of the FPD controller (blue solid lines) are compared with the closed-loop outputs of the DD controller (magenta dashed-dotted lines) in Fig. 5. The two controllers reject the disturbance in the plasma current I_p quickly and drive the I_p around the constant reference (feedforward) value when the boundary ι profile reaches the target, as shown in Fig. 5 (a). Beam and gyrotron powers, shown in Fig. 5 (c)-(l), are weakly modulated by the DD model-based controller within the saturation limits, but strongly controlled by the FPD model-based controller. When the whole ι profile, especially the inner part of ι profile, reaches the target in the end of the simulation, H&CD powers are driven by the FPD controller close to the reference (feedforward) values . After the disturbances especially with Δu_{d_2} are applied, the inputs of some gyrotrons and the 210L NBI reach saturation and activate the anti-windup compensator as shown in Fig. 5 (d), (f), (g) and (k). The electron density is not controlled by the DD controller, so u_n is the same as the reference input. The FPD model includes the electron density model, which gives the new capability to control the density, as shown in Fig. 5 (b).

V. CONCLUSION

A first-principles-driven, model-based, multi-input-multi-output (MIMO), ι profile controller has been designed for the H-mode discharges in DIII-D. The control design is based on the control-oriented model introduced in the companion paper [8]. The feedback controller can regulate the system to the target, even in the presence of various disturbances. Singular value decomposition of the steady state transfer function is used to decouple the system in steady state and identify the most relevant control channels. The mixed

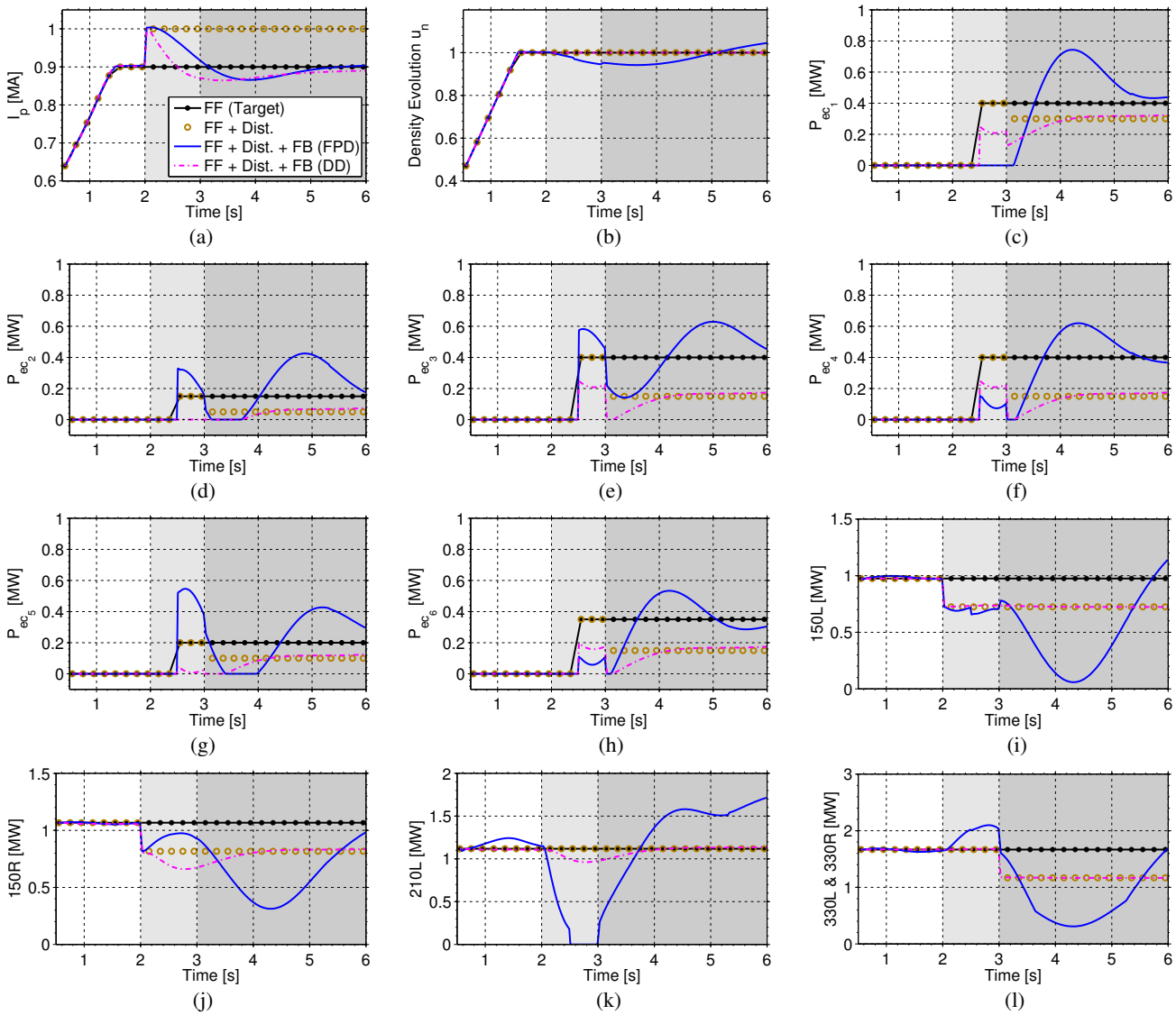

Fig. 5. Rotational transform ι profile closed-loop simulated inputs for each actuator: Reference (feedforward) inputs (black solid-dotted lines), feedforward inputs with disturbances (brown circle line), feedforward+feedback control by First-principles-driven (FPD) controller (blue solid lines), and feedforward+feedback control by Data-driven (DD) controller (magenta dashed-dotted lines). Light-gray background: feedback on - Disturbance I on, dark-gray background: feedback on - Disturbance II on, white background: feedback on - disturbance off.

sensitivity H_∞ technique is used to minimize the tracking error and to optimize control effort. When compared with the control performance of a previous data-driven model-based current profile controller, the proposed first-principles-driven model-based H_∞ controller shows potential for improving control regulation in the inner part of the ι profile.

REFERENCES

[1] Y. Ou *et al.*, "Towards Model-based Current Profile Control at DIII-D," *Fusion Engineering and Design*, vol. 82, pp. 1153–1160, 2007.

[2] E. Witrant *et al.*, "A control-oriented model of the current profile in tokamak plasma," *Plasma Physics and Controlled Fusion*, vol. 49, pp. 1075–1105, 2007.

[3] F. Felici *et al.*, "Real-time physics-model-based simulation of the current density profile in tokamak plasmas," *Nuclear Fusion*, vol. 51, no. 083052, 2011.

[4] C. Xu, J. Dalessio, Y. Ou *et al.*, "Ramp-Up Phase Current Profile Control of Tokamak Plasmas via Nonlinear Programming," *IEEE Transactions on Plasma Science*, vol. 38, no. 2, pp. 163–173, 2010.

[5] J. Barton, M. Boyer, W. Shi, E. Schuster *et al.*, "Toroidal Current Profile Control During Low Confinement Mode Plasma Discharges in DIII-D via First-Principles-Driven Model-based Robust Control Synthesis," *Nuclear Fusion*, vol. 52, no. 123018, 2012.

[6] M. Boyer, J. Barton, E. Schuster, and M. Walker, "Backstepping Control of the Plasma Current Profile in the DIII-D Tokamak," in *Proceedings of the 2012 American Control Conference*, 2012.

[7] M. Boyer, J. Barton, E. Schuster *et al.*, "First-principles-driven model-based current profile control for the DIII-D tokamak via LQI optimal control," *Plasma Physics and Controlled Fusion*, vol. 55, 2013.

[8] J. Barton, W. Shi *et al.*, "Physics-based Control-oriented Modeling of the Safety Factor Profile Dynamics in High Performance Tokamak Plasmas," *Proceedings of the 52nd IEEE International Conference on Decision and Control*, 2013.

[9] G. Ambrosino, M. Ariola, and A. Pironti, "Optimal Steady-state Control for Linear Non Right-invertible Systems," *IET Control Theory and Applications*, vol. 1, no. 3, pp. 604–610, 2007.

[10] W. Shi, W. Wehner, J. Barton *et al.*, "System Identification and Robust Control of the Plasma Rotational Transform Profile and Normalized Beta Dynamics for Advanced Tokamak Scenarios in DIII-D," *submitted to Nuclear Fusion*, 2012.

[11] F. Hinton *et al.*, "Theory of plasma transport in toroidal confinement systems," *Rev. Mod. Phys.*, vol. 48, pp. 239–308, 1976.

[12] R. Hawryluk, "An Empirical Approach to Tokamak Transport," in *Course on Physics of Plasma Close to Thermonuclear Conditions, Varenna, Italy*, 1979.